Bioimaging of uranium and thorium in mice organs by laser ablation inductively coupled plasma mass spectrometry

Xiaoyun Li[1,2] · Xiaomei Wang[3] · Jing Zhou[1] · Zi-Jian Li[1] · Linjuan Zhang[1,2] · Jian-Qiang Wang[1,2]

Abstract

The spatial distribution of thorium, uranium and other radioactive elements in biological tissues is significant for evaluating their migration, toxicity and possible decorporation mechanism, however, it is still a big challenge today for developing quantitative imaging by laser ablation inductively coupled plasma mass spectrometry (LA-ICP-MS) due to the lack of matrix matched standards for calibration. Herein, a fast and reliable LA-ICP-MS quantitative imaging method was developed by using gelatin plus standard solution to prepare a self-made reference material containing 100 μg/g of U and Th, overcoming the inhomogeneity of the raw animal tissue standard. Then the elemental spatial distribution of kidney and liver tissues from mice were revealed by using LA-ICP-MS method. The results showed that U accumulated mainly in the kidney and slightly in the liver, while most of Th was distributed in the liver and few of that in kidney. It was found that U and Th were heterogeneously distributed in kidney section while homogeneously distributed in liver section.

Introduction

Radioactive elements are widely distributed in nature and exist in ores, soil, natural water, and atmosphere. Human activities, such as mining, nuclear processing and agriculture, can alter their geological distribution and release them into the environment, resulting in health risks [1]. Uranium (U) and thorium (Th) are considered global environmental contaminants due to their radioactivity and chemical toxicity. There are different routes to introduce U and Th into the human body, such as through ingestion, inhalation and wound-related absorption, and their risk to human health arises from their ability to accumulate in human tissues.

Significant accumulation of U in the kidneys, spleen, thymus and sternum of mice can be observed after 4 months of U-containing feed [2]. Th exposure study in mice showed that thorium stimulates the damage of lung, liver, and kidney by changing the antioxidant system [3].

Information on the spatial distribution of elements is important for understanding their migration, toxicity mechanism and other effects in organisms, and studies related to biological imaging have received great attention [4, 5]. Various bio-imaging techniques have been used to the study of the spatial distribution of elements, such as synchrotron radiation micro-X-ray fluorescence (SR-μXRF) [6], secondary ion mass spectrometry (SIMS) [7], particle-induced X-ray emission with microprobe (μ-PIXE) [8], and laser ablation-inductively coupled plasma-mass (LA-ICP-MS) [9–11]. The detection limits of μ-PIXE and μ-XRF were 1–10 μg/g and 0.1–1 μg/g, and the spatial resolutions were 0.2–2 μm and 0.1–1 μm, respectively [12], however, their applications are limited by the accessibility of the equipment and the operating cost. Quantitative SIMS analysis is difficult due to matrix effects and polyatomic ion interference. In addition, sample preparation for SIMS, μ-PIXE and μ-XRF requires much effort due to need to operate under high vacuum. In contrast, LA-ICP-MS, which can provide

✉ Linjuan Zhang
zhanglinjuan@sinap.ac.cn

✉ Jian-Qiang Wang
wangjianqiang@sinap.ac.cn

1 Key Laboratory of Interfacial Physics and Technology, Shanghai Institute of Applied Physics, Chinese Academy of Sciences, Shanghai 201800, China

2 University of Chinese Academy of Sciences, Beijing 100049, China

3 Soochow University, Suzhou 215123, China

multi-element detection with significantly spatial resolution (normally 5–150 μm [12]) and high sensitivity, is relatively inexpensive, and the instrumental operation and sample preparation are much simpler. In recently years, LA-ICP-MS has been widely used to study local distribution of essential or toxic elements such as copper (Cu), iron (Fe), cadmium (Cd), silver (Ag), and lead (Pb), and U of various biological samples [9, 10, 13–18]. Studies have shown that LA-ICP-MS has higher sensitivity than SR-μXRF when applied to imaging tungsten (W) and zinc (Zn) in bone tissue of mice [15], as well as La_2O_3 nanoparticles in plant leaves [17].

One of the main challenges for quantitative imaging of biological tissue by LA-ICP-MS is the lack of matrix matched standards for calibration. The number of commercially available matrix matched multi-element standard is very limited. A research focused on the study of the U content in different regions of mouse kidney sections with LA-ICP-MS, used prepared external standards using homogenized chicken liver as a substrate, but no information regarding the imaging of kidney sections was provided [18]. Another study proposed quantitative imaging of rat kidney sections by LA-ICP-MS using thulium-spiked gelatin as an internal standard and homogenized U-added rat kidney as an external standard [9]. The preparation of standards from raw animal tissues was time-consuming, the homogeneity was disputable, while the complex preparation process could also reduce the reproducibility and traceability of the obtained standards [9, 18]. Therefore, there is an urgent need for fast and reliable multi-element reference materials. Gelatin-based standards can be easily prepared and can simulate the properties of the biological tissues, facts which make them suitable to be used as standard matrix. Due to element-dependent heterogeneity in the preparation of gelatin-based films, the distribution of elements in gelatin standards may be uneven. It was demonstrated that heterogeneity problems that might occur while preparing gelatin based multi-element calibration standards can be overcome by optimizing the drying/setting conditions [19]. Within the mentioned study, it was developed a homogeneous, matrix-matched standard preparation procedure for quantitative LA-ICP-MS imaging of protein samples of animal or human origin.

The homogeneity of U/Th spiked standards using gelatin and feasibility for LA-ICP-MS imaging of animal tissues has not been thoroughly studied until the present moment. And there has not yet been any procedure using LA-ICP-MS to obtain the distribution of Th in animal tissues. In addition, small areas (e.g., < 1 mm scale) analyzed by LA-ICP-MS may differ significantly from the concentration of the whole organ, thus bioimaging the larger areas (whole organ sections, cm scale) would be more significant. Therefore, this study proposes a rapid and simple quantitative imaging method of using LA-ICP-MS to image U and Th in the whole sections of mouse tissues. Multi-element standards, including U and Th, were prepared on gelatin matrix, and their accuracy and homogeneity were evaluated. LA-ICP-MS parameters such as laser energy, scan speed, and washout time were optimized to acquire the distribution of U and Th in whole kidney thin sections (approximately 0.7×1.1 cm) within 3 h. To further verify its feasibility, we also imaged Fe, Cu and Zn in kidney sections, as well as U and Th in liver sections.

Experimental

LA-ICP-MS imaging

A double-focusing sector field inductively coupled plasma mass spectrometer (Attom, Nu instrument, Wrexham, UK) with a 193 nm ArF excimer-based laser ablation system (LA, excite, Teledyne Photon Machines, USA) was used for all the analysis. The LA system was equipped with a HelEx two-volume ablation cell (Teledyne Photon Machines, USA), which was coupled to the ICP torch. The ICP-MS and the LA unit operated synchronously in external trigger mode, and the two-volume ablation cell with an aerosol rapid introduction system can improve the resolution of element imaging. High purity helium (99.999%) was used as carrier gas to deliver the aerosol generated at the ablation site on the sample surface to the ICP-MS. Before entering the ICP-MS system, the He gas flow was mixed with high purity argon (99.999%) make-up gas flow. The time-resolved analysis (TRA) mode was used in all experiments, and 10 s gas blank signal was recorded before each line scan to establish the baseline level. Instrumental and optimized experimental parameters for LA-ICP-MS bioimaging are summarized in Table 1.

Routine performance check and fine tuning of the LA-ICP-MS system was performed by ablating NIST 610 reference material (National Institute for Standards and Technology, USA) to ensure maximum U signal intensity and a U/Th signal ratio close to 1. Self-made gelatin standards (see below) were used for calibration and instrument drift compensation. Two replicate line scans of the gelatin standard were performed before and after the analysis of tissue section samples. To obtain two-dimensional images of the elemental distribution, tissue sections of mice (see below) were ablated progressively in a unidirectional line scan mode with no space between lines. Raw data were imported into the Iolite software (v 4.0) and converted into images. The length and width of the ablation areas were set in the software to obtain images with accurate shape.

Table 1 Instruments and optimized experimental parameters

LA-ICP-MS		
ICP-MS instrument	ATTOM (Nu instrument, UK)	
	Plasma RF power	1300 W
	Cooling gas	14 L/min
	Auxiliary gas	0.6 L/min
	Make-up gas	0.5 psi
	Scanning mode	Linked scan
	Acquisition cycle	0.22 s
	Mass resolution	$m/\Delta m = 300$
	Monitored isotopes	^{28}Si, ^{57}Fe, ^{63}Cu, ^{66}Zn, ^{232}Th, ^{238}U
LA instrument	Analyte excite (Teledyne Photon Machines, USA)	
	Laser	ArF Excimer Laser
	Wavelength	193 nm
	Laser energy	2 mJ
	Laser spot size	50 µm
	Scan speed	200 µm/s
	Repetition rate	20 Hz
	Carrier gas	0.6 L/min
	Pulse length	< 4 ns
	Washout time	0.9 s

Gelatin standard

Multi-element calibration standards of 100 µg/g U and Th were prepared employing a similar process proposed by Šala et al. [19]. A mixture of 0.2 g gelatin (porcine-skin gelatin, type A, bloom strength 300, Sigma-Aldrich, USA), 20 µL of U standard solution (1000 µg/mL, SPEX CertiPrep, USA), 20 µL of Th standard solution (1000 µg/mL, SPEX CertiPrep, USA), and Milli-Q water (18.2 MΩ·cm, Millipore, France) were added to a 2 mL tube, and a homogeneous 10% (m/v) spiked gelatin solution was made at 65 °C for 30 min. Hot gelatin solutions (20 µL each) were carefully drop-casted onto adhesion microscope slides (CITOTEST, China) using a Gilson micropipette, and the slides were transferred to a petri dish and dried at 100 °C for 1 h in a mechanical convection oven (XMTD-8222, Shanghai JingHong Laboratory Equipment Co., China). The prepared gelatin standards were stored at 4 °C before use. To determine the average concentrations of U and Th, gelatin standards were digested with 2 ml 68% HNO_3 at 65 °C using a graphite digestion device for 30 min and analyzed by solution ICP-MS.

Biological samples preparation

The Female Kunming mice (6–8 weeks, 30 ± 2 g) were used for the in vivo biodistribution assays. All animal assays were approved by the Animal Care and Use Committee of Soochow University and were conducted in according to the National Institutes of Health guidelines. These animals were intravenously injected with uranyl nitrate solution or thorium nitrate solution (15 mg/kg body weight) and sacrificed 3 h after the injection. The kidney and liver were collected from the uranium and thorium exposed mice, respectively, and then fixed in formalin, embedded in optimal cutting temperature compound (OCT), and cut into 50 µm-thick sections on a cryostat (Leica CM1900). The obtained cryo-sections were mounted directly onto adhesion microscope slides (Shitai, China) and stored at −20 °C until used for LA-ICP-MS analysis. Among these samples, the kidney from one of the U-exposed mice was used for the repeatability experiment of the LA-ICP-MS imaging method. Quantitative elemental imaging experiments were performed on the kidneys and livers of two other mice exposed to U or Th.

Results and discussion

Evaluation of the gelatin standards

The gelatin reference material is prepared by dropping the hot spiked gelatin solution onto a glass slide. Due to the so-called "Marangoni" effect or "coffee stain" effect [19] and the possibility of loss or contamination of added elements, the homogeneity of element distribution and the accuracy of element concentration in the gelatin standards are of vital importance.

Four dried gelatin standards (see Fig. 1a) with a diameter of about 6 mm were randomly line-scanned (length 2.5 mm) to study the distribution of U and Th in gelatin. The gelatin standards were thick enough (~ 100 µm) that only their surfaces were ablated. The profiles of the signal intensity of U and Th, which were relatively stable, were illustrated in Fig. 1b. The signal relative standard deviations (RSDs) of gelatin standards were calculated and listed in Fig. 1c. As can be seen, for the four gelatin standards tested, the average RSDs of the signal intensities of U and Th in one-line scan were 10.8 and 13.0%, respectively, and for their average signal intensities, the RSDs were 1.9 and 2.7%, respectively. These results indicated that the gelatin standards had good homogeneity and reproducibility, in comparison with the gelatin standards that were presented in [20]. In the above-mentioned case, a mold-prepared procedure was needed, such that to improve the uniformity of the standards. In this experiment, adhesive microscope slides were used, as it was previously found that dried gelatin films were easily detached from normal glass slides, and the obtained dry gelatin films were essentially round (see Fig. 1a), although the shape of the gelatin droplets appeared hemispherical due to the presence of surface tension. This approach was much simpler and ensured sufficient homogeneity.
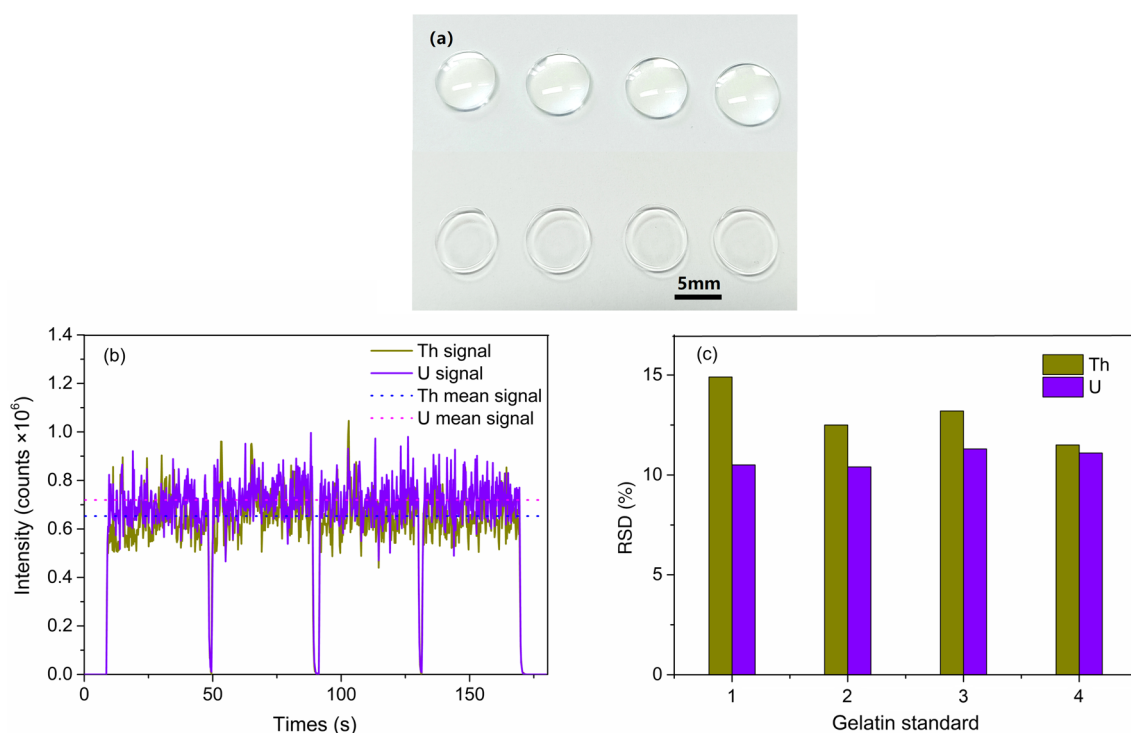
Fig.1 Photographs of gelatin (**a**) before (top row) and after (bottom row) drying, intensity profiles (**b**) and RSDs (**c**) of U and Th for line-scanned gelatin standards

To quantify the concentrations of U and Th in the self-made gelatin standards, four gelatin standards were digested with concentrated HNO_3 and determined by solution ICP-MS. The U concentration and Th concentration in the spiked gelatin standards were 104 ± 2 µg/g and 102 ± 4 µg/g, indicating that the recoveries were both close to 100% and that there was essentially no contamination or loss of the target elements during the preparation of the standards.

Optimization of LA-ICP-MS parameters

Spatial resolution, sensitivity and analysis time are key factors for the quality of LA-ICP-MS imaging, and they are mainly affected by analysis parameters such as laser spot size, laser energy, scan speed and washout time. In this study, the laser energy and scanning speed were investigated by ablating kidney tissue sections, while the washout time was searched using the self-made gelatin standards. The optimized parameters have been shown above in Table 1.

The laser energy affects the depth of ablation and determines whether the sample can be effectively ablated. Lower laser energy may result in lower signals, due to the smaller amount of ablated material obtained, while higher laser energy may lead to complete penetration of the sample or larger material deposition on the sample surface, resulting in contamination and affecting the results of the elemental distribution analysis [13]. To evaluate the laser energy

conditions, two adjacent lines (2 mm each) in the same region of a kidney tissue section were ablated with 50 µm laser spot size, 50 µm/s scan speed, and 20 Hz repetition rate. Three consecutive laser line scans were carried out on each line. For the laser energy of 3 mJ, the U signal of the second laser scan dropped sharply to 2.7% of the first laser scan (see Fig. 2a), indicating that the tissue section was completely penetrated during the first laser scan. The small U signal at the second laser scan was most likely caused by the redeposition of a fraction of the ablated particles on the sample surface [21]. Moreover, the signals of ^{28}Si measured at the first and the second laser scan (see Fig. 3a) were of the same order as those on the glass slide (see Fig. 3b, purple line), which indicated that the glass slide was probably ablated at the first laser scan in this case. On the other hand, when the laser energy was 2 mJ, the U signals tended to decrease more slowly, and the signal intensity of the second scan reached 14.2% of the first scan (see Fig. 2b). In addition, the signal of ^{28}Si at the first ablation were in the same order as that of the background of the carrier gas mixed with the make-up gas (data not shown). These results indicated that the laser energy of 2 mJ ensures adequate ablation of tissue sections with minimal ablation of the glass slides.

The laser spot size is directly related to the signal intensity and the resolution. Due to the increase of the ablation amount of the material, the signal intensity (sensitivity) of the analyzed element increases with the increase of the laser
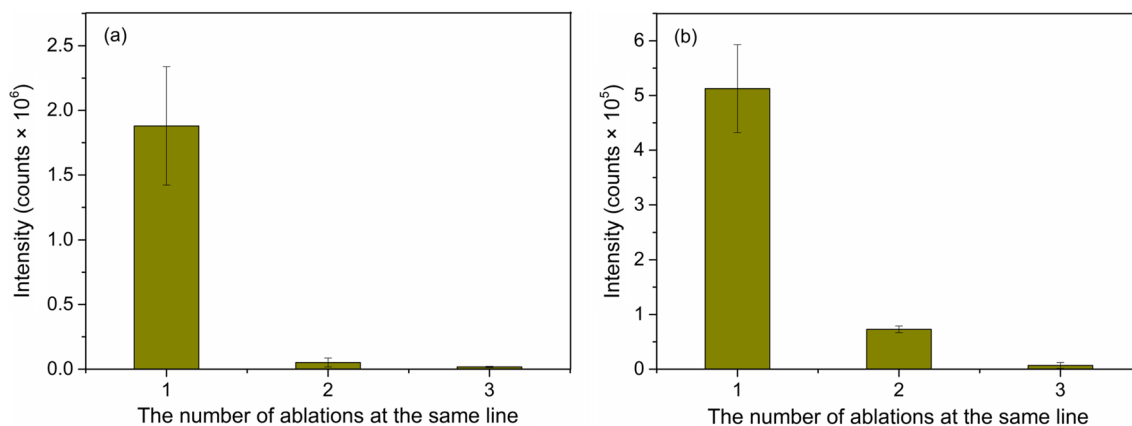
Fig. 2 The intensity of U corresponding to the number of ablations at the same line for 3 mJ (**a**) and 2 mJ (**b**). Error bars 1SD
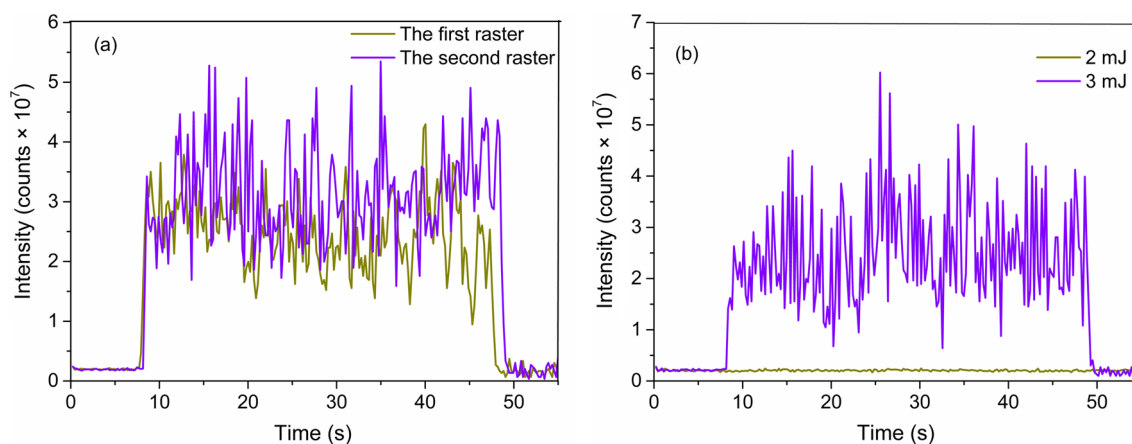

Fig. 3 Signal profiles of ^{28}Si obtained by LA-ICP-MS line scan. (**a**) line scan of kidney tissue section on the same line at laser energy of 3 mJ, (**b**) line scan of glass slide at different laser energies

spot size. Scan speed has a direct influence on the resolution. The reduction in laser spot size and scan speed will lead to longer analysis time, which not only increases the analysis cost, but also leads to signal instability or instrumental drift, while the image resolution may not be significantly improved [22]. Generally, the imaging spatial resolution of LA-ICP-MS in biological samples is in the range of $5 \sim 150$ μm [12]. A laser spot size of 50 μm was chosen in all the experiments to ensure sufficient imaging resolution and keep the total analysis time within a reasonable range. Imaging experiments were performed on areas of 1.5 mm × 1.5 mm at scan speeds equal to 1, 2, 3, 4 and 5 times of the laser spot size per second, using 2 mJ laser energy, 50 μm spot size, and 20 Hz repetition rate. When the spot size, scan area, acquisition cycle and other parameters are constant, the scan speed affects the number of data points (one pixel represents one data point), thus affecting the number of pixels and resolution. At scan speeds of 50 and 100 μm/s, as shown in Fig. 4(a) and (b), more data points were acquired,

resulting in images with more pixels and higher resolution. In Fig. 4 (c–e), the shape of each pixel was closer to a square at scan speeds of 150 and 200 μm/s, while it was a horizontal rectangle when the scan speed was 250 μm/s. When the scan speed is very slow, the total analysis time could be too long and may lead to over-sampling, while too fast a scan speed may lead to data loss and resolution loss [23]. As a result, a scan speed of 200 μm/s was chosen for subsequent experiments to compromise the imaging resolution and the analysis time. In this study, if the total analysis time for a whole kidney tissue section were to become longer, it would introduce uncertainties caused by instrument signal drift due to the lack of a suitable internal standard.

The imaging quality of LA-ICP-MS is also affected by the washout time of the ablation cell, which is calculated from the transient signal, that is, the time required for the signal to go from 100 to 1% after the laser stops firing [24]. A "blurred" image may arise from increased washout time, which increases the interference of the signal from the
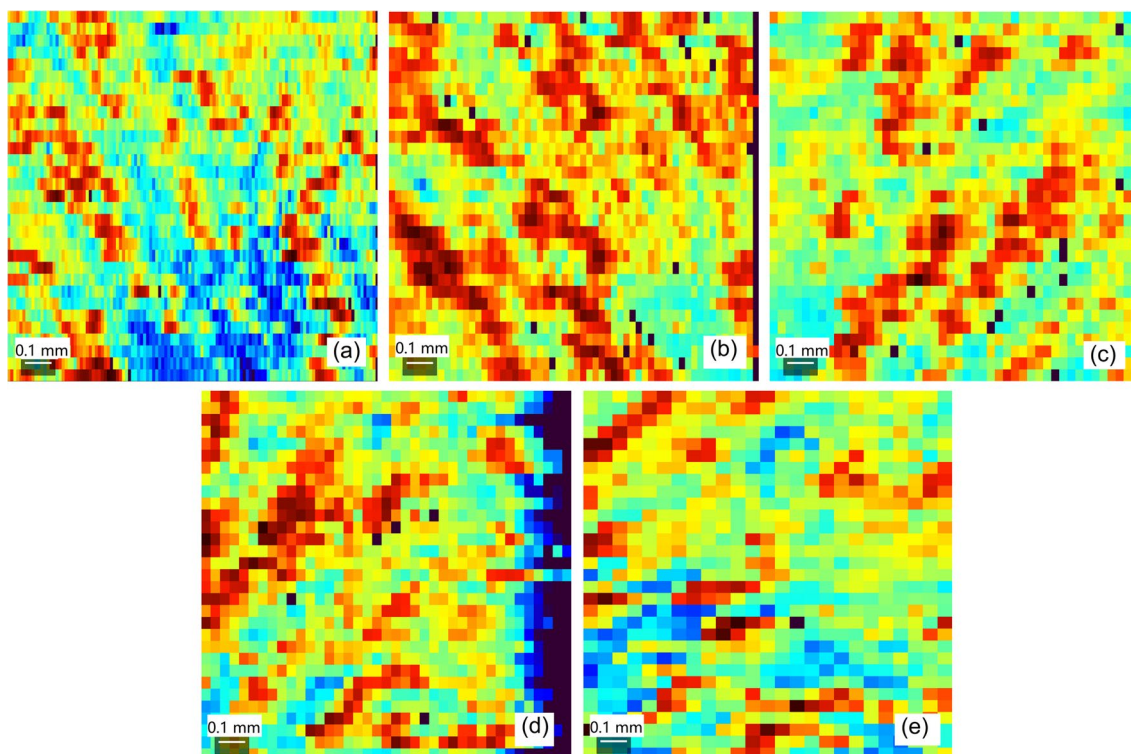
Fig. 4 U images were obtained at different scan speed: (**a**) 50 μm/s; (**b**) 100 μm/s; (**c**) 150 μm/s; (**d**) 200 μm/s; (**e**) 250 μm/s. Scale bars = 0.1 mm
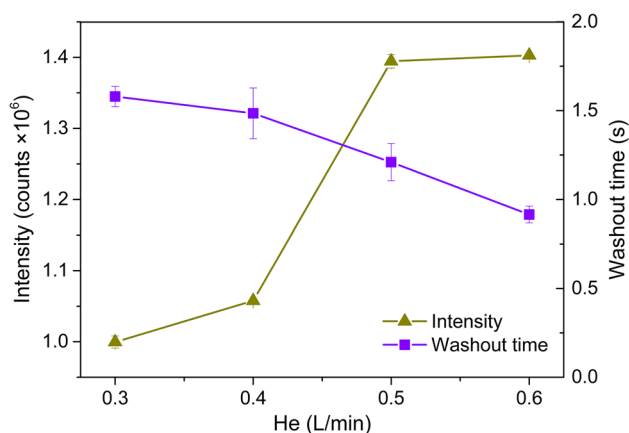
Fig. 5 Effect of He flow rate on U signal intensity and washout time. Error bars 1SD

previous data point on the next data point. In this study, the washout time as a function of He flow rate was assessed by analyzing the U signal in the two-volume ablation cell. It can be seen from Fig. 5 that as the He flow rate increased from 0.3 to 0.6 L/min, the washout time gradually decreased from 1.6 to 0.9 s, while the U signal increased rapidly due to the increase of sample transfer rate, and it was relatively stable when He flow rate was greater than 0.5 L/min, indicating

that almost all the aerosols generated by laser ablation were delivered to the detector. Therefore, the He flow rate was set at 0.6 L/min. The washout time of the ablation cell used in this study was equivalent to or slightly better than most of commercial applied ablation cells [25, 26].

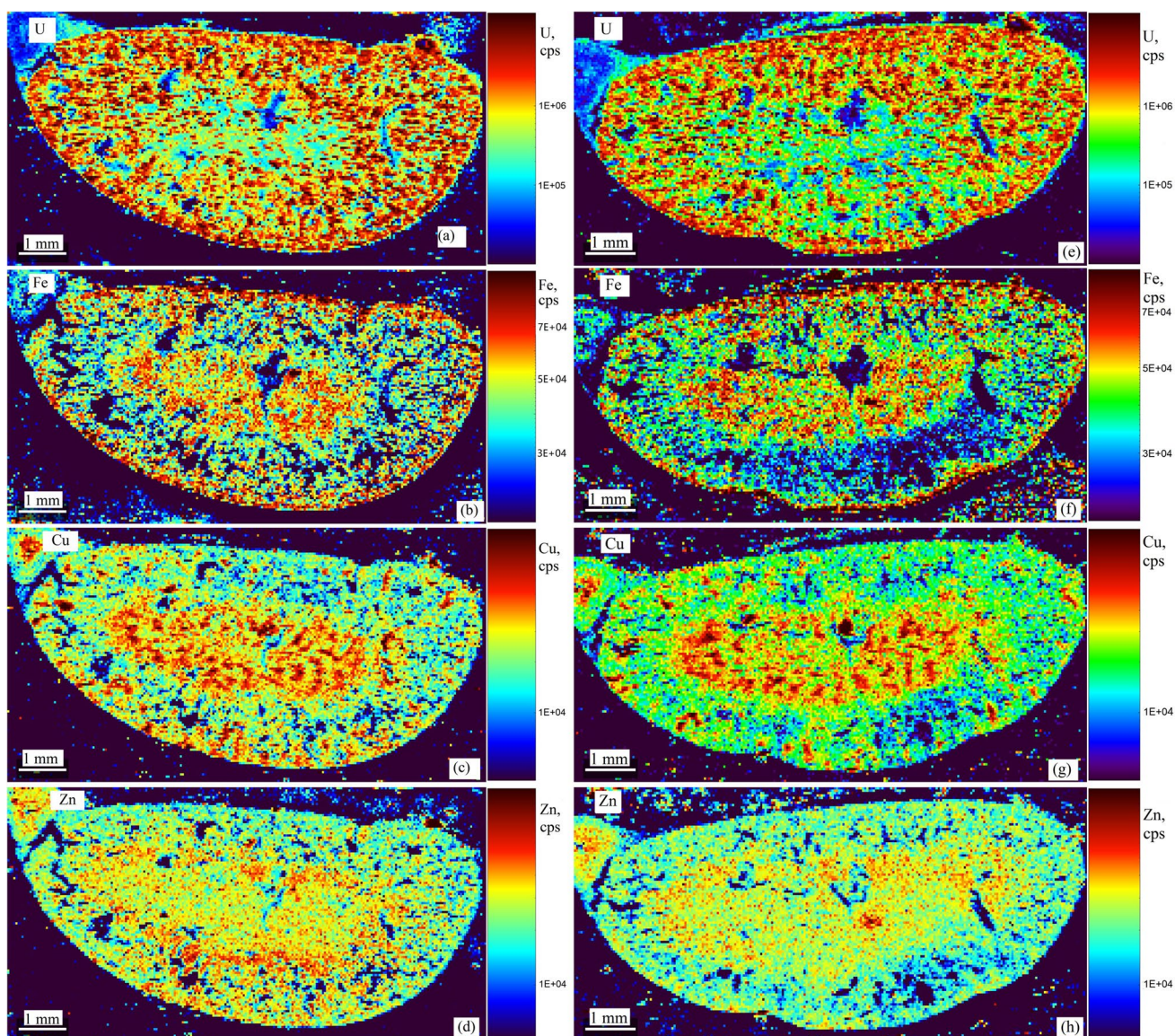## Repeatability of the LA-ICP-MS bioimaging method

Using the optimized instrumental parameters described above, the imaging analysis of a whole kidney tissue section can be completed in a relatively short time of about 3 h, which can prevent signal drift of the instrument. To verify the reliability of these parameters, the repeatability of U imaging was studied by analyzing two sections of the same kidney from one mouse injected with U. Moreover, the distribution of the essential elements such as Fe, Cu and Zn that were of great concern in the kidney sections were also investigated simultaneously to further display the capability of the LA-ICP-MS for multi-element imaging under the same condition. Because of their unique importance for life, elemental imaging of Fe, Cu and Zn can provide crucial information. Moreover, it has been shown that the ingestion of heavy metals may lead to changes in the distribution of these essential elements in tissues, so it is of interest to image these essential elements simultaneously in future

experiments to investigate the biochemistry of uranium and thorium [27–29].

Images based on the raw signal intensity were produced for each of the measured elements. The results, as shown in Fig. 6, indicated that the images of each element exhibit certain patterns and the resolution obtained can clarify the distribution of these elements in the kidney structure. By comparing the results from the replicated sections (U-1 and U-2) of the same kidney, it can be found that the distribution and signal intensity of U, Fe, Cu and Zn in both sections were similar, respectively, and their expected slight differences may be due to the heterogeneity of the organ. The results demonstrated that the elemental imaging was reproducible under the optimized conditions obtained above.

The element images also showed that elements were not uniformly distributed in the kidney tissue of mouse, and the distribution of U in the kidney differed from that of essential elements. To date, several studies have investigated the distribution of nutrient elements in the kidney of mice exposed to U. In this study, Fe was mainly distributed in the medulla and outermost layer of the cortex, Cu was mainly distributed in the medulla, and Zn tended to accumulate in the outer stripe of medulla and the inner stripe of the cortex. It has been reported that after exposure to U, Fe was localized in the inner stripe of the outer medulla, and Zn was uniformly distributed in the cortex and the outer stripe of the outer medulla [29]. Exposure to U contamination will affect Fe metabolism and change the distribution of Fe in the kidney

Fig. 6 Evaluation of the LA-ICP-MS bioimaging method. Element images of replicate tissue sections U-1 (**a**, **b**, **c**, **d**) and U-2 (**e**, **f**, **g**, **h**) of the same kidney of the mouse exposed to U. The color scales indicate the obtained signal intensities in cps

[27]. Studies have shown that Fe deposition in renal medulla of mice increased significantly after exposure to depleted uranium [27, 28]. However, the distribution results of Fe and Cu were inconsistent with previous studies of normal mouse kidneys measured by μ-XRF [30]. This study would contribute to further understanding of the mechanism of U toxicity. Although multi-elements simultaneous imaging can be considered as a great challenge for biological image acquisition, the developed LA-ICP-MS bioimaging method was reliable and can be used for multi-element analysis of kidney sample at tissue level.

Quantitative bioimaging of U and Th

Quantitative imaging of kidney and liver sections from U-exposed or Th-exposed mouse were studied using self-made gelatin standards by a one-point calibration method. Quantitative results were obtained by comparing the signal intensities of the elements in samples and standards containing 100 μg/g U and Th, respectively. Carbon was not used as an internal standard in the quantification because the signals of carbon were different in tissue and gelatin, and it is not uniformly distributed in tissues. Moreover, it has been shown that carbon was not an ideal internal standard for bioimaging because the ablation behavior of carbon containing samples was complex [31]. As shown in Fig. 7, the images obtained under the optimized conditions of this study clearly showed the heterogeneous distribution of U and Th in the whole kidney tissue section, respectively.

According to previous studies, U accumulates mainly in the outer medullary region and proximal tubules of mice kidneys, which locate mainly in the cortex [32]. In the whole kidney tissue section of Fig. 7a, the average U concentration was 331 μg/g. Six areas (0.2–0.5 mm^2) were randomly selected in the cortex and medulla, respectively, and the average U concentrations were 317 ± 40 μg/g and 194 ± 61 μg/g, indicating that the average U concentration in the cortex was almost twice as high as that in the medulla. However, the average U concentration in eleven random locations in the highly concentrated areas was 4300 ± 1448 μg/g, which was up to 13-fold higher compared with the whole kidney tissue section U concentration. The U concentration in the highly concentrated locations, i.e., the proximal tubule of the inner zone of the cortex and in the outer strip of the outer medulla, could even be as high as 6602 μg/g. These results were consistent with the data obtained in previously published reports [33–35]. SR-μXRF and μXAFS analysis of U accumulation in the kidneys of rats exposed to uranyl acetate (0.5 mg/kg body weight) also showed that U was distributed in the inner cortex and outer stripe of the outer medulla of the kidney, and in one U-concentrated area, a maximum U concentration of 959 μg/g was measured [6]. Using SR-XRF to determine U accumulation in the kidneys of U exposed mice, it was found that after subcutaneous injection of 2 mg U/kg uranium acetate for 3 h, U was mainly distributed in the proximal tubule of the inner zone of the cortex and in the outer stripe of the outer medulla [33]. In particular, the results of Fig. 7a were in excellent agreement with the quantitative results obtained by Grijalba [9] using LA-ICP-MS, which used both thulium-added gelatin as an internal standard and homogenized U-spiked rat kidney as external standards, while the quantification method used in this study was much simpler.
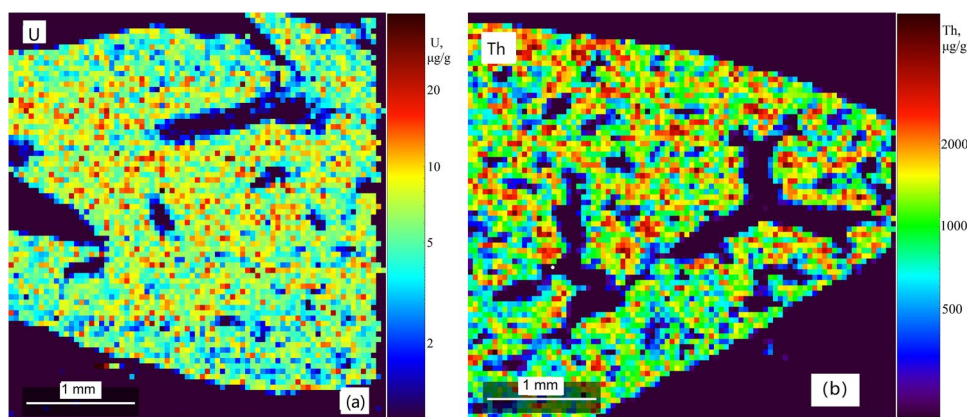
On the other hand, the average Th concentration in the whole kidney tissue section was only 36 μg/g (see Fig. 7b). Similarly, for six randomly selected areas in the cortex and

Fig. 7 Elemental distribution images on kidney tissue sections from mouse exposed to U (**a**) or Th (**b**)
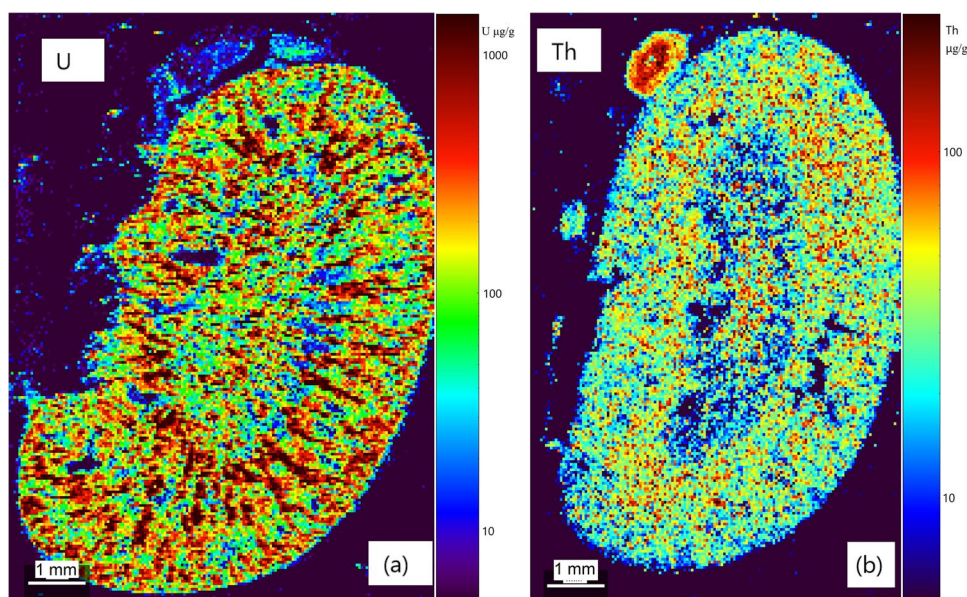
Fig. 8 Elemental distribution images on liver tissue sections from mouse exposed to U (**a**) or Th (**b**)

medulla, respectively, the average Th concentrations were 36 ± 6 µg/g and 21 ± 4 µg/g, thus the Th concentration in the cortex was nearly twice as high as the Th concentration in the medulla, which is similar to the trend of U obtained in the present study. However, it was clear that although both the injection of U and Th were 15 mg/kg body weight, the concentration of U in the kidney was an order of magnitude higher than that of Th, which was consistent with the fact that the kidney is the target organ for the accumulation of element U.

On the contrary, the concentrations of U and Th in the liver sections of mice sections had opposite trends (see Fig. 8). The concentrations of U and Th in the liver of U-exposed and Th-exposed mice were approximately 7 µg/g and 1300 µg/g, respectively. Moreover, unlike in the mice kidney sections, there were no specific pattern in the images of U and Th in the liver sections, suggesting that the distribution of U and Th in the liver was relatively homogeneous. This may be related to the fact that anatomically and physiologically, the liver is considered to be a homogeneous organ. The elemental distribution results were consistent with previously reported elemental imaging results of Pb exposed mice [12].

Conclusions

A new method based on LA-ICP-MS was developed and applied to the elemental imaging of tissue sections of mice exposed to U or Th. U and Th spiked gelatin was used as the standard material, and the effects of parameters such as laser energy, scan speed and washout time on the lateral resolution were investigated. Elemental imaging of U, Fe, Cu and Zn in parallel samples demonstrated that the new method has excellent repeatability and can clearly showed the inhomogeneous distribution of these elements. Quantitative imaging proved that U accumulated mainly in the kidney and slightly in the liver, while Th accumulated mainly in the liver and few in the kidney. In conclusion, we reported for the first

time that U and Th exhibit similar distribution trend in the kidney sections of mice. Quantitative imaging analysis of tissue sections of U or Th exposed mice using LA-ICP-MS helps to further understand the effect of U or Th on the biochemical metabolism of mice. Further studies on the biochemical behavior under conditions of long-term exposed of low doses of U or Th are underway in our laboratory.

Declarations

Conflict of interest The authors declare that they have no conflict of interest.

References

1. Pereira R, Barbosa S, Carvalho FP (2014) Uranium mining in Portugal: a review of the environmental legacies of the largest mines and environmental and human health impacts. Environ Geochem Health 36:285–301. https://doi.org/10.1007/s10653-013-9563-6
2. Hao Y, Ren J, Liu J, Yang Z, Liu C, Li R, Su Y (2013) Immunological changes of chronic oral exposure to depleted uranium in mice. Toxicology 309:81–90. https://doi.org/10.1016/j.tox.2013.04.013
3. Chaudhury D, Sen U, Sahoo BK, Bhat NN, Kumara KS, Karunakara N, Biswas S, Shenoy PS, Bose B (2022) Thorium promotes lung, liver and kidney damage in BALB/c mouse via alterations in antioxidant systems. Chem Biol Interact 363:109977. https://doi.org/10.1016/j.cbi.2022.109977
4. Francischini DS, Arruda MAZ (2021) When a picture is worth a thousand words: molecular and elemental imaging applied to environmental analysis—A review. Microchem J 169:106526. https://doi.org/10.1016/j.microc.2021.106526
5. Doble PA, de Vega RG, Bishop DP, Hare DJ, Clases D (2021) Laser ablation-inductively coupled Pplasma-mass spectrometry imaging in biology. Chem Rev 121:11769–11822. https://doi.org/10.1021/acs.chemrev.0c01219

6. Homma-Takeda S, Uehara A, Yoshida T, Numako C, Sekizawa O, Nitta K, Sato N (2020) Two-dimensional μXAFS analysis for accumulated uranium in kidneys of rats exposed to uranyl acetate. Radiat Phys Chem 175:108147. https://doi.org/10.1016/j.radphyschem.2019.02.006

7. Tessier C, Suhard D, Rebiere F, Souidi M, Dublineau I, Agarande M (2012) Uranium microdistribution in renal cortex of rats after chronic exposure: a study by secondary ion mass spectrometry microscopy. Microsc Microanal 18:123–133. https://doi.org/10.1017/S1431927611012384

8. Homma-Takeda S, Fujishiro H, Tanaka I, Yakumaru H, Ayama K, Uehara A, Oikawa M, Himeno S, Ishihara H (2021) Single-cell imaging for studies of renal uranium transport and intracellular behavior. Minerals 11:191. https://doi.org/10.3390/min11020191

9. Grijalba N, Legrand A, Holler V, Bouvier-Capely C (2020) A novel calibration strategy based on internal standard-spiked gelatine for quantitative bio-imaging by LA-ICP-MS: application to renal localization and quantification of uranium. Anal Bioanal Chem 412:3113–3122. https://doi.org/10.1007/s00216-020-02561-4

10. Togao M, Nakayama SMM, Ikenaka Y, Mizukawa H, Makino Y, Kubota A, Matsukawa T, Yokoyama K, Hirata T, Ishizuka M (2020) Bioimaging of Pb and STIM1 in mice liver, kidney and brain using Laser Ablation Inductively Coupled Plasma Mass Spectrometry (LA-ICP-MS) and immunohistochemistry. Chemosphere 238:124581. https://doi.org/10.1016/j.chemosphere.2019.124581

11. Halbach K, Wagner S, Scholz S, Luckenbach T, Reemtsma T (2019) Elemental imaging (LA-ICP-MS) of zebrafish embryos to study the toxicokinetics of the acetylcholinesterase inhibitor naled. Anal Bioanal Chem 411:617–627. https://doi.org/10.1007/s00216-018-1471-2

12. Jurowski K, Buszewski B, Piekoszewski W (2015) The analytical calibration in (bio)imaging/mapping of the metallic elements in biological samples–definitions, nomenclature and strategies: state of the art. Talanta 131:273–285. https://doi.org/10.1016/j.talanta.2014.07.089

13. Pessoa GS, Lopes Junior CA, Madrid KC, Arruda MAZ (2017) A quantitative approach for Cd, Cu, Fe and Mn through laser ablation imaging for evaluating the translocation and accumulation of metals in sunflower seeds. Talanta 167:317–324. https://doi.org/10.1016/j.talanta.2017.02.029

14. Ralbovsky NM, Zou L, Chen B, Zhang NR, Hines CDG, Vavrek M, Zhong W, Smith JP, Bu X (2021) Simultaneous multielement imaging of liver tissue using laser ablation inductively coupled plasma mass spectrometry. Talanta 235:122725. https://doi.org/10.1016/j.talanta.2021.122725

15. VanderSchee CR, Kuter D, Chou H, Jackson BP, Mann KK, Bohle DS (2020) Addressing K/L-edge overlap in elemental analysis from micro-X-ray fluorescence: bioimaging of tungsten and zinc in bone tissue using synchrotron radiation and laser ablation inductively coupled plasma mass spectrometry. Anal Bioanal Chem 412:259–265. https://doi.org/10.1007/s00216-019-02244-9

16. Weller A, Zok D, Steinhauser G (2019) Uptake and elemental distribution of radiosilver [108m]Ag and radiocesium ^{137}Cs in shiitake mushrooms (Lentinula edodes). J Radioanal Nucl Chem 322:1761–1769. https://doi.org/10.1007/s10967-019-06778-1

17. Neves VM, Heidrich GM, Rodrigues ES, Enders MSP, Muller EI, Nicoloso FT, Carvalho HWPd, Dressler VL (2019) La_2O_3 nanoparticles: study of uptake and distribution in Pfaffia glomerata (Spreng.) Pedersen by LA-ICP-MS and μ-XRF. Environ Sci Technol 53:10827–10834. https://doi.org/10.1021/acs.est.9b02868

18. Jim V, LaViolette C, Briehl MM, Ingram JC (2017) Spatial distribution of uranium in mice kidneys detected by laser ablation inductively coupled plasma mass spectrometry. J Appl Bioanal 3:43–48. https://doi.org/10.17145/jab.17.007

19. Sala M, Selih VS, van Elteren JT (2017) Gelatin gels as multi-element calibration standards in LA-ICP-MS bioimaging: fabrication of homogeneous standards and microhomogeneity testing. Analyst 142:3356–3359. https://doi.org/10.1039/c7an01361b

20. Zhou J, Ni X, Fu J, Li Y, Guo W, Jin L, Hu S (2021) Quantitation and imaging analysis of biological samples by LA-ICP-MS. Atomic Spectroscopy 42(4):210–216. https://doi.org/10.46770/as.2021.068

21. Villaseñor Á, Greatti C, Boccongelli M, Todolí JL (2017) A dried droplet calibration approach for the analysis of solid samples through laser ablation—inductively coupled plasma mass spectrometry. J Anal Atom Spectrom 32:587–596. https://doi.org/10.1039/c6ja00343e

22. Moreno-Gordaliza E, Giesen C, Lazaro A, Esteban-Fernandez D, Humanes B, Canas B, Panne U, Tejedor A, Jakubowski N, Gomez-Gomez MM (2011) Elemental bioimaging in kidney by LA-ICP-MS as a tool to study nephrotoxicity and renal protective strategies in cisplatin therapies. Anal Chem 83:7933–7940. https://doi.org/10.1021/ac201933x

23. Lear J, Hare D, Adlard P, Finkelstein D, Doble P (2012) Improving acquisition times of elemental bio-imaging for quadrupole-based LA-ICP-MS. J Anal Spectrom 27:159–164. https://doi.org/10.1039/c1ja10301f

24. Cole LM (2017) Imaging mass spectrometry. Name Humana Press, New York

25. Vaculovič T, Warchilová T, Čadková Z, Száková J, Tlustoš P, Otruba V, Kanický V (2015) Influence of laser ablation parameters on trueness of imaging. Appl Surf Sci 351:296–302. https://doi.org/10.1016/j.apsusc.2015.05.136

26. Li Q, Fang Y, Liu J, Zhang C, Wang Z (2021) Elemental imaging of alumina ceramic tube using laser ablation- inductively coupled plasma-mass spectrometry (LA-ICP-MS). Atom Spectrosc 42:154–159. https://doi.org/10.46770/as.2021.019

27. Berradi H, Bertho J-M, Dudoignon N, Mazur A, Grandcolas L, Baudelin C, Grison S, Voisin P, Gourmelon P, Dublineau I (2008) Renal anemia induced by chronic ingestion of depleted uranium in rats. Toxicol Sci 103:397–408. https://doi.org/10.1093/toxsci/kfn052

28. Donnadieu-Claraz M, Bonnehorgne M, Dhieux B, Maubert C, Cheynet M, Paquet F, Gourmelon P (2007) Chronic exposure to uranium leads to iron accumulation in rat kidney cells. Radiat Res 167:454–464. https://doi.org/10.1667/RR0545.1

29. Terada Y, Homma-Takeda S, Takeuchi A, Suzuki Y (2010) High-energy X-Ray microprobe system with submicron resolution for X-Ray fluorescence analysis of uranium in biological specimens. X-Ray Opt Instrument 2010:1–5. https://doi.org/10.1155/2010/317909

30. Li C, Xu W, Chu S, Zheng Z, Xiao Y, Li L, Bi H, Wei L (2018) The chemical speciation, spatial distribution and toxicity of mercury from Tibetan medicine Zuotaibeta-HgS and HgCl2 in mouse kidney. J Trace Elem Med Biol 45:104–113. https://doi.org/10.1016/j.jtemb.2017.08.010

31. Frick DA, Günther D (2012) Fundamental studies on the ablation behaviour of carbon in LA-ICP-MS with respect to the suitability as internal standard. J Anal Atom Spectrom 27:1294. https://doi.org/10.1039/c2ja30072a

32. Sabolić I (2006) Common mechanisms in nephropathy induced by toxic metals. Nephron Physiol 104:107–114. https://doi.org/10.1159/000095539

33. Homma-Takeda S, Terada Y, Nakata A, Sahoo SK, Yoshida S, Ueno S, Inoue M, Iso H, Ishikawa T, Konishi T, Imaseki H, Shimada Y (2009) Elemental imaging of kidneys of adult rats exposed to uranium acetate. Nucl Instrum Meth B 267:2167–2170. https://doi.org/10.1016/j.nimb.2009.03.082

34. Homma-Takeda S, Kokubo T, Terada Y, Suzuki K, Ueno S, Hayao T, Inoue T, Kitahara K, Blyth BJ, Nishimura M, Shimada Y (2013) Uranium dynamics and developmental sensitivity in rat kidney. J Appl Toxicol 33:685–694. https://doi.org/10.1002/jat.2870

35. Homma-Takeda S, Numako C, Kitahara K, Yoshida T, Oikawa M, Terada Y, Kokubo T, Shimada Y (2019) Phosphorus localization and its involvement in the formation of concentrated uranium in the renal proximal tubules of rats exposed to uranyl acetate. Int J Mol Sci 20:4677. https://doi.org/10.3390/ijms20194677